Small-number statistics near the clustering transition in a compartmentalized granular gas

René Mikkelsen,[1,2] Ko van der Weele,[1] Devaraj van der Meer,[1] Martin van Hecke,[2] and Detlef Lohse[1]
[1]*Department of Science and Technology and J. M. Burgers Centre for Fluid Dynamics, University of Twente, P. O. Box 217, 7500 AE Enschede, The Netherlands*
[2]*Kamerling Onnes Laboratory, P. O. Box 9504, 2300 RA Leiden, The Netherlands*
(Received 2 December 2004; published 8 April 2005)

Statistical fluctuations are observed to profoundly influence the clustering behavior of granular material in a vibrated system consisting of two connected compartments. When the number of particles N is sufficiently large ($N \approx 300$ is sufficient), the clustering follows the lines of a standard second-order phase transition and a mean-field description works. For smaller N, however, the enhanced influence of statistical fluctuations breaks the mean-field behavior. We quantitatively describe the competition between fluctuations and mean-field behavior (as a function of N) using a dynamical flux model and molecular dynamics simulations.

DOI: 10.1103/PhysRevE.71.041302 PACS number(s): 45.70.−n, 05.40.−a, 05.70.Jk

I. INTRODUCTION

Clustering is one of the most characteristic features of granular gases, arising from the inelastic collisions between the particles, and making them fundamentally different from any ordinary molecular gas. The clustering phenomenon was first observed in molecular dynamics (MD) simulations of a freely cooling gas, consisting of inelastically colliding particles in the absence of gravity and energy input [1]. Every particle was given an initial velocity and after a number of collisions, a separation into dense and dilute regions set in. Since collisions are more frequent in dense regions and hence the dissipation is stronger there, ultimately almost all the particles were seen to accumulate in clusters of slow particles. The intermediate regions were depleted, containing only a few (but relatively fast) particles.

More recently, the clustering phenomenon has been studied also in driven (vibrofluidized) granular gases. A particularly clear-cut illustration of the effect is found when the system is divided into two equally sized compartments separated by a wall of finite height [2–6]. This type of geometry enables a straightforward quantification of the clustering process by counting the number of particles in each compartment at a given time. Pictures taken from experiments in such a setup are shown in Fig. 1. At strong shaking [Fig. 1(a)] the particles spread equally over the two compartments, just as in any ordinary molecular gas. However, when the shaking strength is reduced below a critical threshold [Figs. 1(b)–1(d)], the particles cluster into one of the two compartments. A steady asymmetric configuration is reached in which one compartment contains many slow particles, and the other compartment only a few, but rapid ones. When the shaking strength is decreased further, the configuration gradually becomes more asymmetric.

A quantitative model for the clustering of a granular gas in such a compartmentalized system was derived by Eggers [3], based on a statistical description of the energy budget within the gas. Central in this model is a flux function, which represents the flow of particles between the compartments: The flux out of compartment i ($i=1,2$), containing a fraction n_i of the total number of particles in the system, is given by the function $F(n_i)$. The dynamics of the model is then governed by the following balance equation [3,4]:

$$\frac{dn_1}{dt} = -F(n_1) + F(n_2) + \xi_1, \tag{1}$$

i.e., the change in the particle fraction in compartment 1 is equal to the mean flux it receives from compartment 2 [$F(n_2)$], minus the mean flux leaving compartment

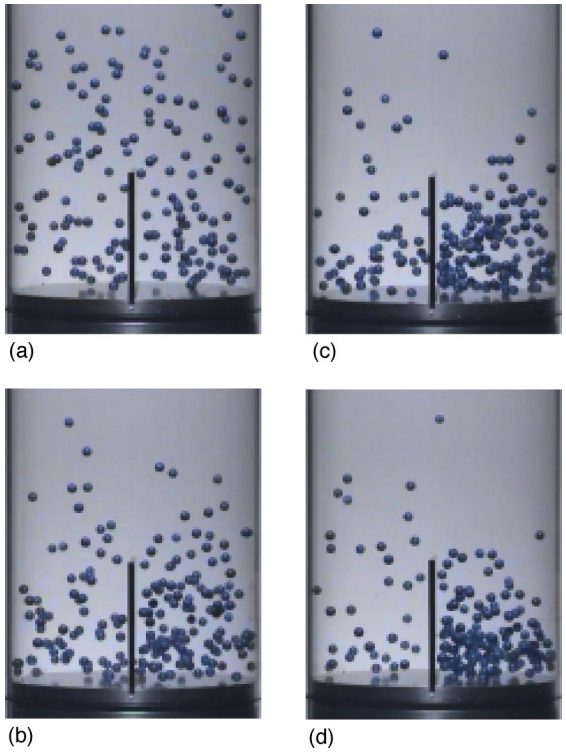

FIG. 1. Experimental snapshots from a clustering experiment in a compartmentalized container with $N=300$ glass beads. At strong shaking (amplitude $a=1.0$ mm, frequency $f=70$ Hz) the particles are distributed evenly over the two compartments (a). When the shaking strength is reduced ($a=1.0$ mm, $f=50$ Hz) an asymmetric clustered state is seen to develop (b)–(d). The pictures are taken 5 (b), 10 (c), and 25 s (d) after reducing the shaking strength.

1 $[F(n_1)]$. The last term ξ_1 is the noise term, which is generally assumed to be Gaussian and white [3,7,8].

Due to particle conservation $(n_1+n_2=1)$ the dynamics given by Eq. (1) can be rewritten as

$$\frac{dn_1}{dt} = G(n_1) + \xi_1, \tag{2}$$

where $G(n_1)=-F(n_1)+F(1-n_1)$ is the net mean flux out of compartment 1. So far the focus has been on systems containing a large number of particles, for which the statistical noise constitutes only a relatively small perturbation to the mean-field behavior governed by $G(n_1)$. For such systems, the Eggers flux model has proven to describe the clustering transition very well, not only for a two-compartment system but also for the generalized case of $k>2$ connected compartments [4–6]. In this paper, however, we will reduce the particle number to such an extent that the influence of the noise term becomes comparable to (or even stronger than) the mean-field behavior. Thus we witness how the mean-field phase transition gives way to its noise-dominated counterpart. At sufficiently high noise rates (i.e., small particle number N) the transition is completely wiped out and no clustering occurs anymore.

The compartmentalized gas at hand (like many other granular systems) is inherently noisy, owing to the fact that it contains *much* fewer particles than the typical 10^{23} from textbook statistical physics. This makes it a very natural and suitable model system to study the influence of statistical fluctuations on critical phenomena [9–11]. It may be taken to represent a much wider class of systems with a limited number of particles. In particular, the results of the present study are expected to hold (qualitatively) also for the clustering transition in related granular systems such as the horizontally shaken setup introduced by Brey *et al.* [12,13].

Formally, a phase transition (and the existence of a critical point) is defined only in the limit $N\to\infty$, but here we will use the same terminology also in the more intuitive context of finite-size systems.

We will study the granular gas by means of molecular dynamics simulations. To connect the MD data to the dynamical model, we discretize Eq. (2):

$$\frac{n_i(t+dt)-n_i(t)}{dt} = G(n_i(t)) + \xi(n_i(t)), \tag{3}$$

which, if we take dt equal to the periodicity of the shaking (and take this period as the unit of time, so $dt=1$), can be written as

$$n_i(t+1) = n_i(t) + M(n_i(t)) + \xi(n_i(t)). \tag{4}$$

Here the notation $M(n_i(t))$ [instead of $G(n_i(t))$] is adopted to stress that we are now dealing with the discrete-time mapping from stroke to stroke. To obtain M and ξ from the MD simulations, one simply counts the number of particles that changes compartment during one complete shaking cycle: the average corresponds to M [which may be directly compared with the net flux $F(n_i)$ according to Eggers' theory], and the fluctuations define ξ. We will in particular study the case of small total particle number N, down to $N=50$. The dynamics given by Eq. (4) has the advantage over Eq. (2) that it is easier to implement the constraint on n_i to take on only positive integer values, and it more naturally captures the small-number noise.

Moreover, since in the present context the number of particles is a crucial parameter, we will work mostly with the actual particle numbers N_i (with $N_1+N_2=N$) instead of the particle fractions n_i, which conceal the actual numbers. Of course, the two notations can be translated into one another via $n_i=N_i/N$.

The paper is constructed as follows. Section II gives the MD results for the different (uniform and clustered) shaking regimes, and describes how the nature of the clustering transition changes for decreasing particle number N. In Sec. III the mapping Eq. (4) is reconstructed from the MD data, i.e., both the mean-field term M and the fluctuation term ξ. In Sec. IV we introduce a potential related to M, which enables a direct comparison between the strengths of M and ξ. In Sec. V we then describe the time correlations in the signal $n_i(t)$, one of the key indicators of a critical point in the theory of phase transitions, and used here to illustrate the breakdown of the mean-field behavior for small N. Finally, Sec. VI contains concluding remarks.

II. MD SIMULATIONS

A. Numerical scheme

The molecular dynamics simulations are based on a code that updates the particle and bottom positions every 10^{-5} s. Between collisions, the particles move freely, describing parabolic paths under the influence of gravity. Whenever a particle-particle or particle-wall collision takes place, signaled by a spatial overlap, the velocity vector of the involved particles after collision is computed from the vector before collision according to Newton's laws.

The simulated system consists of two connected rectangular compartments of size 2.45×4.90 cm^2, separated from each other along their longest side by a 3 cm high wall. A total number of N particles is distributed over the two compartments and given a random initial velocity following a normal distribution. The particles are chosen to be smooth (no friction) and hard (no deformation) with radius $r=1.25$ mm and are taken to be made of steel, having mass $m=0.0625$ g and coefficient of restitution $e_{\text{particles}}=0.85$. The particle positions are sampled every 0.01 s. Given the typical velocity of the particles (in the order of 1 m/s) this means that a particle travels roughly 1 cm between successive samples. This is a reasonable trade-off between a very fast sampling rate (for which the situation from sample to sample would change only little) and a slow one (for which the simulation would have to run longer).

This procedure gives information not only on the change in the particle distribution, but also on how many particles have changed compartment from $1\to2$ and $2\to1$. As a result, not only the net particle flux $[G(N_1)]$ but also the individual fluxes from compartments 1 $[F(N_1)]$ and 2 $[F(N_2)]$ are obtained.

The side walls enclosing the setup are taken to be infinitely high, so the system has no upper boundary. All walls,

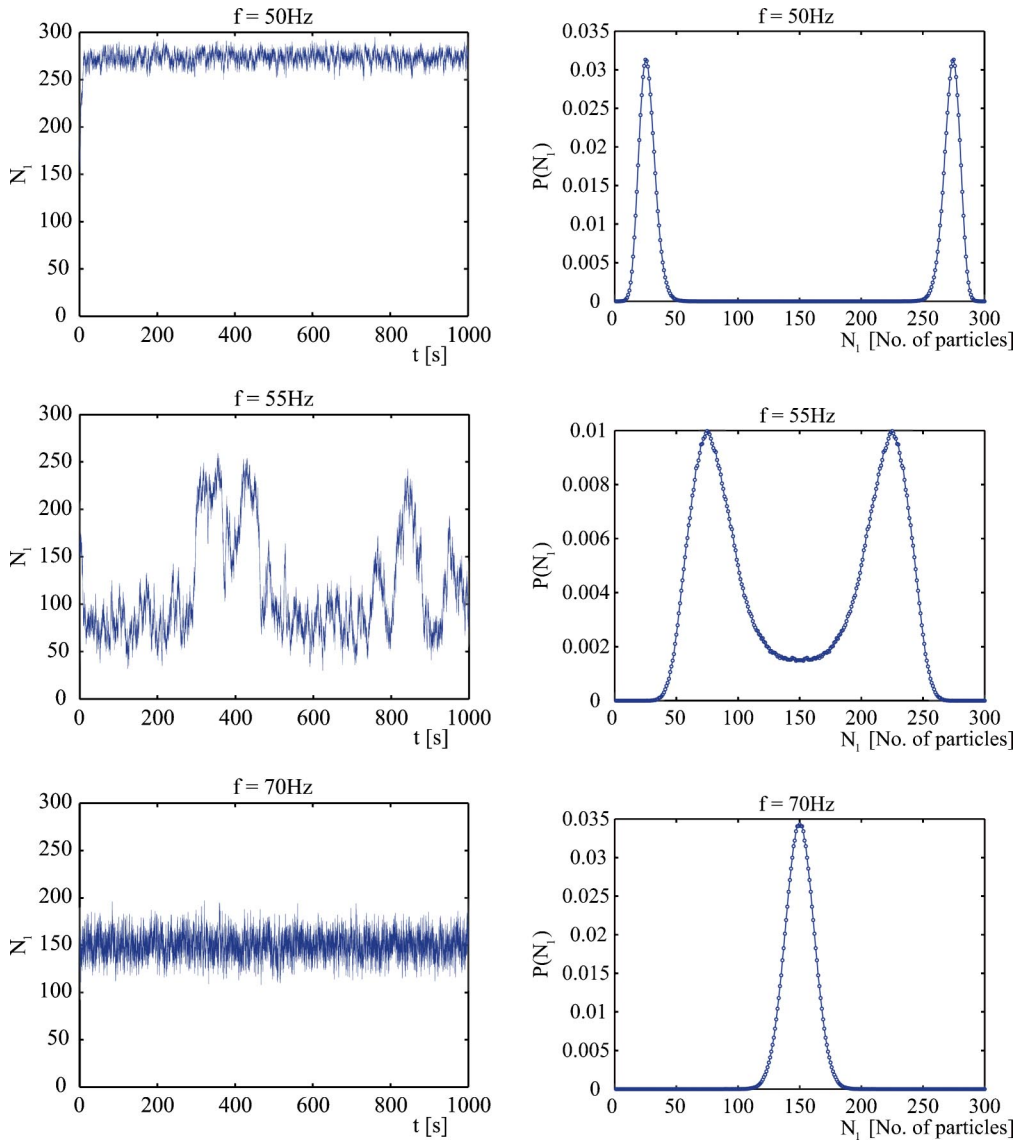

FIG. 2. Molecular dynamics simulations for $N=300$ particles. Left: Time evolution of the number of particles in the left compartment $[N_1(t)]$ starting from the symmetric distribution $N_1(0)=N_2(0)=N/2=150$. Right: Probability distribution function showing the statistical distribution of the particles over the two compartments. Three different regimes are distinguished, depending on the shaking strength. (I) At mild shaking (top, $f=50$ Hz), the particles cluster in one of the two compartments. (II) At intermediate shaking strength (middle, $f=55$ Hz), they still tend to cluster, but the system is intermittently driven out of this state by the statistical fluctuations. (III) For strong shaking (bottom, $f=70$ Hz), the system is fluctuating around the symmetric distribution.

including the bottom, are assigned a coefficient of normal restitution equal to that of glass, $e_{\text{wall}}=0.95$.

Just as in the experiment depicted in Fig. 1, energy is injected into the system by means of a sinusoidally vibrating bottom with adjustable frequency and amplitude. For simplicity, the amplitude is fixed at $a=1$ mm in all simulations presented in this paper, such that the frequency is the only control parameter by which we tune the shaking strength.

B. Time evolution and probability distribution functions

The MD results give a very clear picture of the main phenomenology around the clustering transition. In Fig. 2 (left column) we see how the number of particles evolves in the left compartment as a function of time, for three different frequencies around the critical one. These simulations were done for $N=300$ particles, starting out from the symmetric distribution with $N_1(0)=N_2(0)=150$. The particle distribution was sampled at 100 Hz, and each picture depicts 10^5 samples (10^3 s) in the steady state.

These and similar time series yield the probability distribution function (PDF) shown in the right column of Fig. 2, representing the probability of finding a given number of particles within a compartment. In creating the PDFs the particle numbers for both compartments are used, therefore these are always symmetric around $N/2$ due to particle conservation. The maximum value of the PDF gives the most probable particle distribution and the width of the peaks

around the maximum value is a measure of the magnitude of the fluctuations. The first 10^4 samples (10^2 s) are omitted, in order to avoid initial transients, using the next 10^6 samples (10^4 s) for the determination of the PDFs. The form of the PDFs around the clustering transition has been discussed also in [7], not from molecular dynamics simulations but as the solution of the master equations for a modified version of the Eggers model; and in [8] for the clustering of $N=1000$ granular particles in two connected compartments driven by a stochastic heat bath.

Let us first consider the shaking frequency $f=50$ Hz (Fig. 2, top). The initial symmetric distribution is highly unstable and the particles rapidly cluster into one of the two compartments. The clustered state at $N_1 \approx 275$ is stable and the particle distribution will fluctuate around this value as the shaking is continued. This behavior is reflected in the PDF which has two separate peaks corresponding to the two clustered states, with $N_1 > N_2$ (cluster in left compartment, depicted in the time series plot) and $N_1 < N_2$ (cluster in right compartment), respectively. The maximum and mean values of the peaks are not located at precisely the same position, as the peaks are skewed slightly toward the center $N/2$.

Increasing the shaking strength to $f=55$ Hz shows a change in the behavior of the particle distribution (Fig. 2, middle). The unclustered state still is unstable and the particles rapidly begin to cluster into one of the compartments. However, due to the increased shaking strength (and the fact that the clustered state lies closer to the symmetric state than before) the fluctuations are strong enough to take the system out of this situation and toward the unclustered state again. Since this is unstable, the system quickly evolves back into either one of the two clustered states, giving rise to the intermittent behavior seen in the time series. Looking at the corresponding PDF, two distinct peaks are still present, but they are now connected, in agreement with the observation that the system spends some considerable time in the neighborhood of the unclustered state. The fact that the two peaks have moved closer together illustrates the decreased asymmetry of the clustered state, and their broadening reflects the stronger fluctuations.

For strong shaking, $f=70$ Hz, the only stable configuration is the unclustered state (Fig. 2, bottom). Here the energy input into the system (via the vibrating bottom) overpowers the energy dissipation (via the inelastic collisions) and no clustering occurs. Hence the particle distribution is seen to fluctuate around the unclustered state. The PDF reduces to a single peak, taking the shape of a Gaussian distribution around the unclustered state. Note that the peak is narrower than those for $f=55$ Hz (middle plot): the influence of the fluctuations has decreased again.

C. The clustering transition for varying total particle number *N*

The PDFs obtained for a range of frequencies around the critical value f_c can be used to construct the bifurcation diagrams of Fig. 3. Here we see how the PDF evolves as function of f for three different particle numbers: $N=300$ (top left), 100 (top right), and 50 (bottom left and right). The magnitude of the PDF is indicated by the gray scale, with black corresponding to a low probability ($0.1 < p/p_{\max} \leqslant 0.15$) and white to the highest ($0.95 < p/p_{\max} \leqslant 1$). The (red) backbone curve locates the maximum of the PDF [$p_{\max}(f)$], and the width of the gray-scale area around this curve is directly related to the amplitude of the fluctuations.

For $N=300$ particles the transition between the unclustered and clustered states resembles that of second-order phase transitions known from equilibrium statistical physics, with a characteristic pitchfork bifurcation, branching off as $(f_c - f)^\beta$, with $\beta = \frac{1}{2}$ being the standard mean-field critical exponent [14]. When the critical frequency ($f=f_c \approx 56.7$ Hz) is approached from above, the fluctuations around the (stable) symmetric state grow. Below the critical point ($f < f_c$) the symmetric state is unstable, and it has given way to two asymmetric distributions, one with $N_1 > N_2$ (cluster in the left compartment) and one with $N_1 < N_2$ (cluster in right compartment). These distribution become more asymmetric as f is lowered further away from the critical point f_c, while the fluctuations around the equilibrium decrease. All in all, in this case with relatively many particles the clustering transition is very similar to that predicted by the Eggers model with zero noise [3]. Together with experimental results [4], these MD simulations further validate the Eggers model and its ability to capture the many-particle (mean-field) transition.

Reducing the number of particles in the system causes a change in the transition, since the fluctuations become so strong that they destroy the mean-field characteristics. For $N=100$ particles (Fig. 3, top right) the bifurcation branches are already no longer following the standard square root behavior. Just below $f_c \approx 32$ Hz they stay somewhat closer to the symmetric state, owing to the fact that the fluctuations cause the system to switch intermittently from one clustered state to the other, and in doing so force it to spend some time in the unstable symmetric state as well (cf. the time series in Fig. 2, middle plot).

On the other hand, far away from the critical point the clustering is very pronounced, even more so than in the case of $N=300$ particles. This is due to the small shaking strength here, which leads to an enhanced clustering [3,4].

The breakdown of the mean-field behavior becomes even more evident for $N=50$ (Fig. 3, bottom left). Here we also note that the critical behavior does not actually disappear but is just overwhelmed (and thus made increasingly hard to see) by the large fluctuations. At shaking frequencies above $f_c \approx 26$ Hz, the symmetric state is stable. Upon decreasing the driving frequency below f_c, the particles attempt to cluster in one of the compartments—with many intermittent switches from one compartment to the other—but the branches do not manage to form a fork anymore. In fact, a further decrease of f makes the shaking strength so small that the particles (starting from the symmetric distribution with 25 particles in each compartment) are not able to overcome the separating wall anymore, and they are frozen in the initial state. This also explains the vanishing fluctuations for $f \leqslant 17$ Hz.

If alternatively we start out from the clustered state (with all 50 particles in the left compartment) we get the transition diagram of Fig. 3, bottom right. Up to $f=18$ Hz the particles

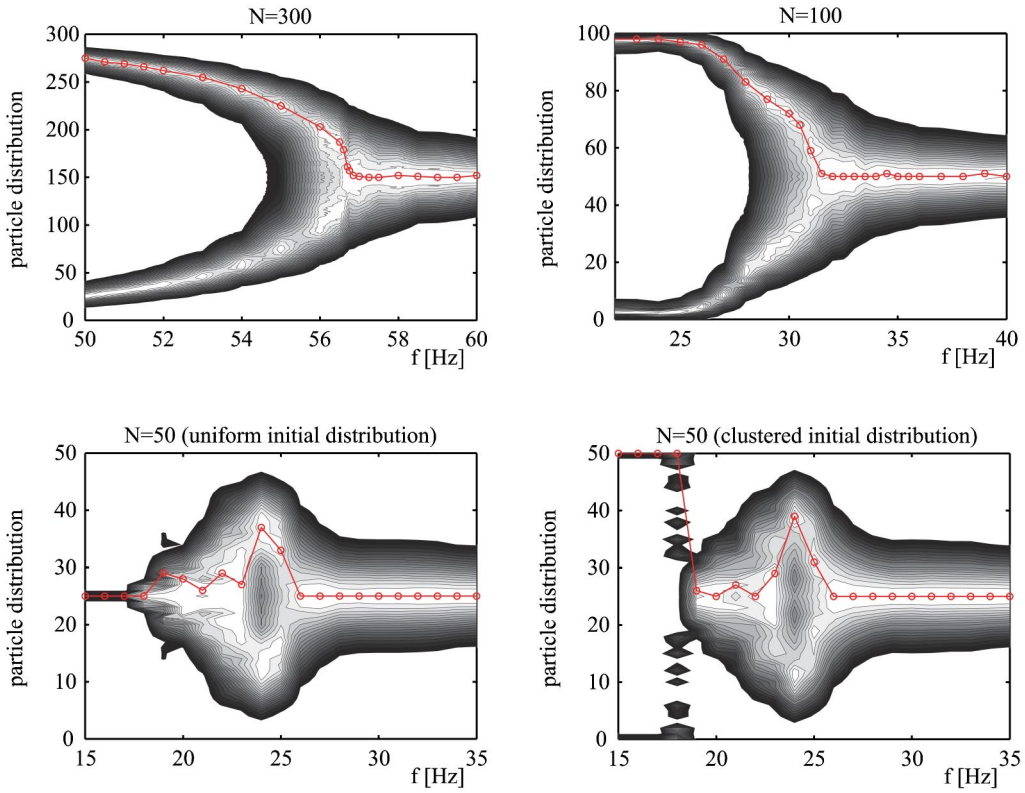

FIG. 3. (Color online) The clustering transition for three different particle numbers: $N=300$ (top left), 100 (top right), and 50 particles [bottom left (starting with both compartments equally filled) and right (starting from a clustered state)]. The contours give the probability. These diagrams are constructed from the PDFs (cf. Fig. 2) for a range of shaking frequencies f around the critical value f_c; the PDFs of Fig. 2 are vertical cuts through this figure. The circles along the backbone curve (red) represent the maximum of the PDF at each measured frequency. For $N=300$ the diagram has all the characteristics of a standard second-order phase transition: a pitchfork bifurcation with its branches opening as $(f_c-f)^{\beta}$, with the mean-field critical exponent $\beta=1/2$. For $N=100$ the branches do not follow this power law anymore due to the increased influence of statistical fluctuations, and for $N=50$ even the branches themselves have deteriorated.

remain frozen in the clustered configuration, followed by a regime where half-grown clusters are intermittently switching from one compartment to the other ($19 \leqslant f \leqslant 25$ Hz), until finally the symmetric distribution becomes stable at $f_c \approx 26$ Hz.

III. CONSTRUCTION OF THE MAP

A. Flux function

We will now proceed to reconstruct the flux function from the MD data, i.e., the outflow of particles from a compartment as a function of its particle content. In contrast to the simulations used to create the time series in Fig. 2, where the particles initially were distributed equally over the two compartments followed by simulating for a long time, this time we sweep through different initial distributions, in order to get sufficient statistics also for the improbable states. The sampling interval is synchronized to the frequency of the shaking, in order to obtain the outflow of particles during one complete shaking cycle, and hence the discrete-time map of Eq. (4).

To justify the form of the mapping in Eq. (4), we measured the correlation between the numbers of particles that change compartment in successive strokes, and found that the outflow in any shaking cycle is indeed uncorrelated to the outflow in the previous stroke. The particle outflow is therefore a Markovian process [10], only depending on the number of particles in the compartment at the start of the shaking cycle (and not on previous particle numbers at earlier strokes).

For every initial distribution, 20 prestrokes are carried out with an infinitely high wall separating the compartments, enabling the particles within each compartment to equilibrate. The wall is then abruptly reduced to 3 cm, after which 20 more strokes are carried out. The results from these last 20 strokes are used to determine the outflow shown in Fig. 4. This procedure is repeated 1000 times (for different initial conditions) to get good statistics.

Figure 4, for $N=300$ particles, contains the results for $f=50$ (top plot), 55 (middle plot), and 70 Hz (bottom plot). As expected the outflow is seen to increase with the shaking strength. The gray scale indicates how probable a given outflow is for a compartment containing N_i particles ($i=1,2$). The (blue) backbone line corresponds to the average outflow of particles, which is the MD analog of the Eggers flux function $F(N_i)$ with zero noise. Just as predicted by Eggers' theory, the average outflow is a one-humped function of N_i,

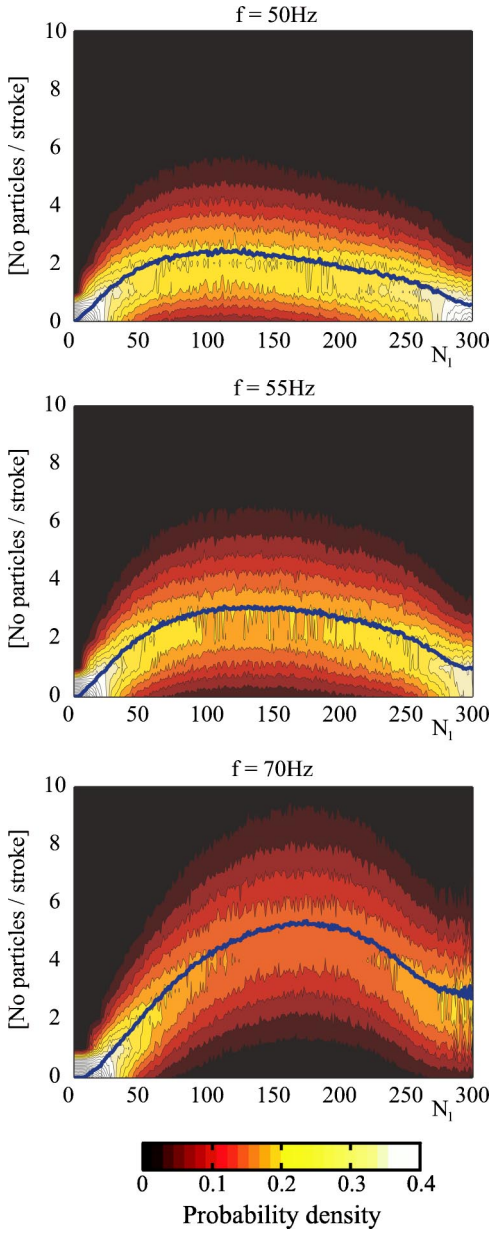

FIG. 4. (Color online) Contour plots showing the probability density of having a given outflow of particles from a compartment as a function of the number of particles N_1 in the compartment, for $f=50$ (upper), 55 (middle), and 70 Hz (lower), all at driving amplitude $a=1$ mm. The probability density has been normalized to 1 for each value of N_1 (integrating along a vertical line in the figure) and its value can be read off from the gray-scale (color) bar. The (blue) backbone line corresponds to the averaged particle flux $F(N_1)$, which can slightly differ from the most probable flux. The plots are based on MD simulations during 20 000 driving strokes.

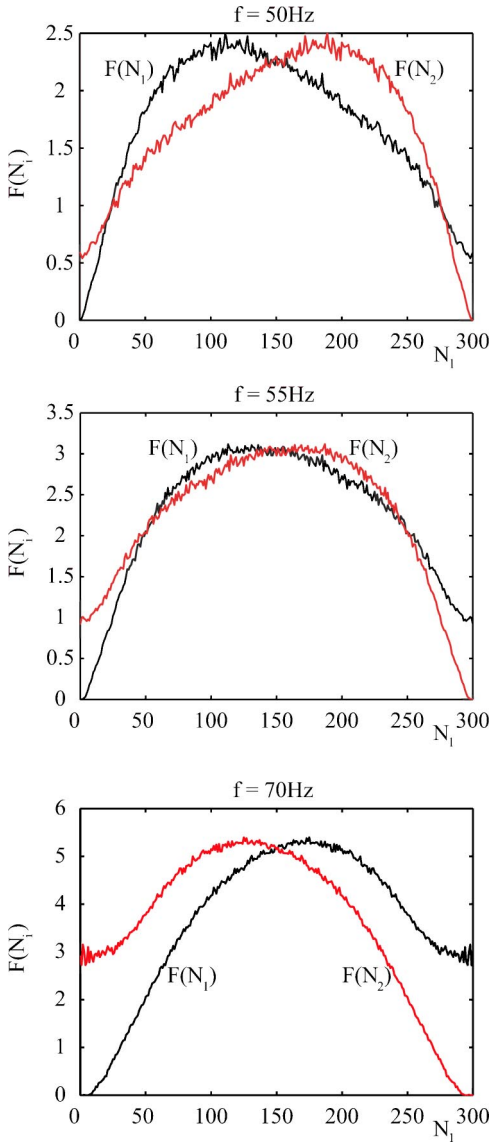

FIG. 5. (Color online) The averaged fluxes $F(N_1)$ (black) and $F(N_2)$ [gray (red)] in a two-compartment system, obtained from MD simulations for $f=50$ (top), 55 (middle), and 70 Hz (bottom) with $a=1$ mm. Where the two curves intersect, the flux of particles out of compartment 1 (black, starting out from zero at $N_1=0$) is balanced by the particles it receives from compartment 2 [gray (red), starting out from zero at $N_1=300$, i.e., $N_2=0$].

which is indeed an essential prerequisite for the clustering phenomenon to occur [3]. However, where the theoretical Eggers function has the form $F(N_i) \propto N_i^2 \exp(-BN_i^2)$, the reconstructed flux function starts out from $N_i=0$ with a power smaller than quadratic. This can be traced back to the fact that in the Eggers theory the dissipation was taken to result from the binary collisions between the particles only (the frequency of which grows as N_i^2), whereas in reality also the collisions of the particles with the walls (linear in N_i) contribute [15]. At low densities ($N_i \to 0$) the particle-wall collisions even become the dominant source of dissipation.

A dynamical equilibrium between the compartments (not necessarily stable) is obtained when the average flux of particles going from $1 \to 2$ is balanced by the flux in the opposite direction $2 \to 1$. In Fig. 5 we therefore plot the averaged flux of particles leaving compartment 1 (starting out from zero at $N_1=0$) together with the flux from compartment 2 (starting out from zero at $N_1=300$, i.e., $N_2=0$): We do so for $f=50$ (top), 55 (middle), and 70 Hz (bottom). Where the two curves intersect the total flux vanishes and the system is in equilibrium.

In the first plot ($f=50$ Hz) *three* equilibrium points can be

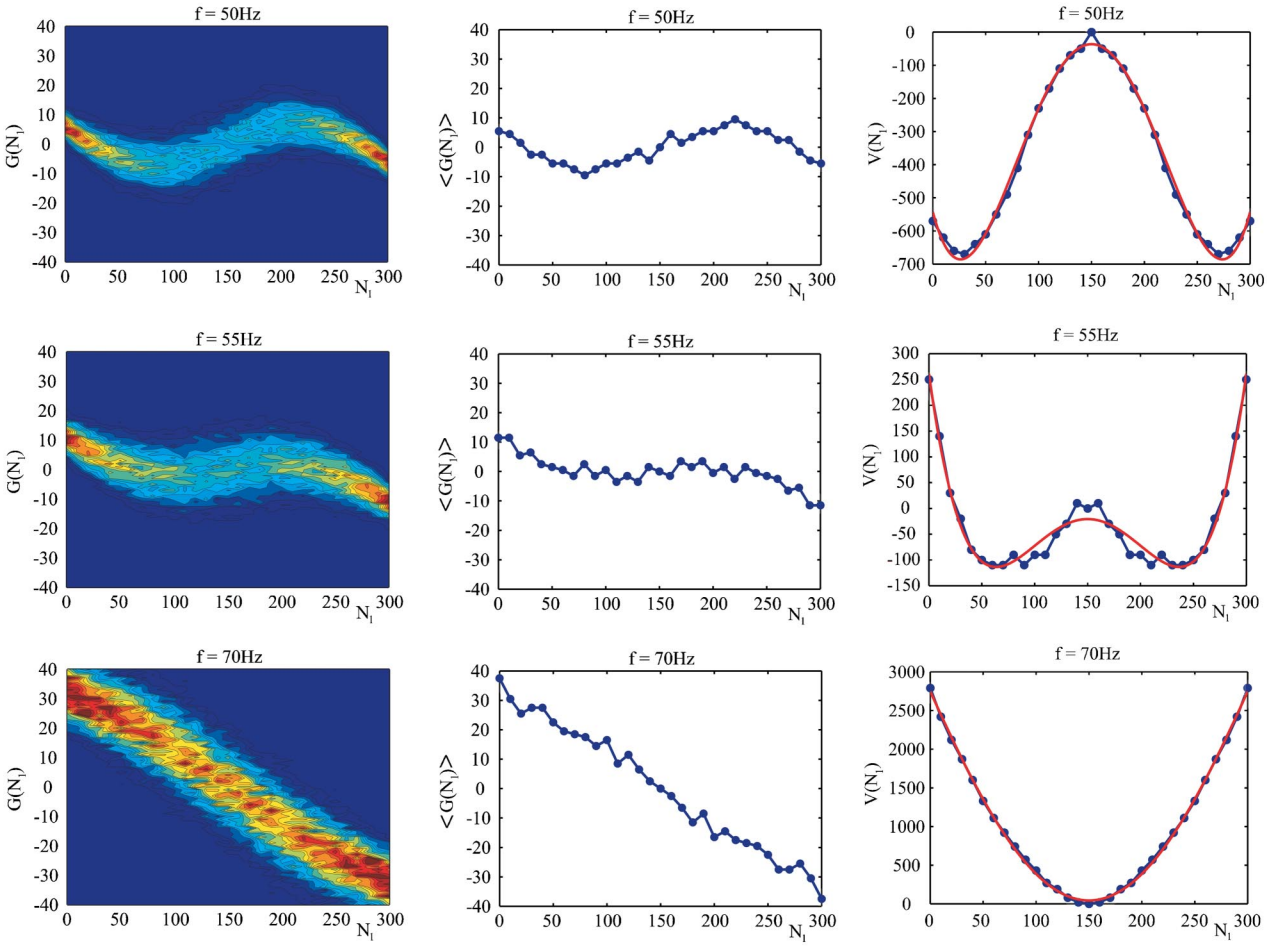

FIG. 6. (Color online) The net flux $G(N)=-F(N_1)+F(N_2)$ (left column) and its average $\langle G(N)\rangle=\langle -F(N_1)+F(N_2)\rangle$ (middle column) obtained from MD simulations for $f=50$ (top), 55 (middle), and 70 Hz (bottom). The amplitude of the driving is $a=1$ mm. The right column shows the potential $V(N_i)$ corresponding to the average net fluxes (see Sec. IV). For mild shaking ($f=50$ Hz, top) the potential consists of two wells (representing the clustered states) separated by a barrier. At the critical shaking frequency (close to $f=55$ Hz, middle) the barrier disappears, and for higher shaking strengths the potential has just one single minimum at the symmetric state $N_i=N/2$ ($f=70$ Hz, bottom). The data have been fitted to a quartic potential as in Eq. (10), with the coefficients $\{V_0,a,b\}$ taking on the values $\{-36.34,-0.0848,2.77\times10^{-6}\}$ for $f=50$ Hz, $\{-20.68,-0.0248,1.16\times10^{-6}\}$ for $f=55$ Hz, and $\{43.48,\ 0.1396,\ 0.87\times10^{-6}\}$ for $f=70$ Hz. Precisely at the critical point, the coefficient a (associated with the quadratic term of the potential) goes through zero.

discerned, corresponding to the (unstable) symmetric distribution $\{N_1=N_2=150\}$ and the two stable clustered states $\{N_1\approx25,N_2\approx275\}$ and $\{N_1\approx275,N_2\approx25\}$. The second plot ($f=55$ Hz) is close to the critical frequency and the three equilibria are on the verge of merging into one, i.e., into the symmetric distribution. In the third plot ($f=70$ Hz) the symmetric equilibrium is the only one left, and has become stable in the process.

B. Stochastic map

In any equilibrium state the net flux $G(N_1)=-F(N_1)+F(N_2)$ is zero. This quantity is shown in Fig. 6 for the same three frequencies as in Figs. 4 and 5. The left column shows the net flux and the right column the averaged function $\langle G(N)\rangle=\langle -F(N_1)+F(N_2)\rangle$. Since we have sampled the flux per stroke of the driving, this averaged net flux is precisely the mean-field term of the mapping introduced in Eq. (4):

$$\langle G(N_i)\rangle = M(N_i). \tag{5}$$

The form of $M(N_i)$ gives information not only about the position of the equilibrium states, but also about their stability. In the clustered regime, $M(N_i)$ takes the form of an S-shaped curve (Fig. 6, top row). Three points of zero net flux exist, corresponding to the two asymmetric equilibria toward the sides (clustered states) and the symmetric distribution in the middle. From the sign of $M(N_i)$ on the intervals between these zeros, it immediately follows that the clustered states are stable and the symmetric one is unstable. For example, for $25\lesssim N_1\lesssim150$, the net flux into compartment 1 is negative: This means that during the following strokes compartment 1 will be depleted even more until it reaches the equilibrium at $N_1\approx25$ where the average net flux vanishes.

Closing in upon the critical frequency, the S-shaped curve is stretched out around the symmetric distribution (Fig. 6,

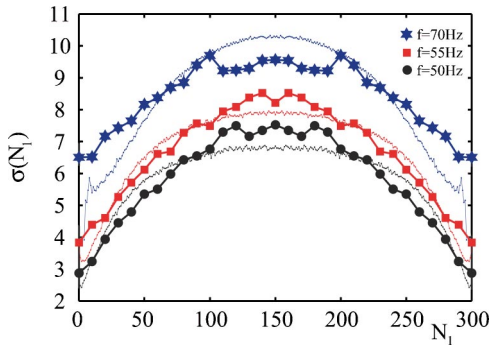

FIG. 7. The standard deviation $\sigma(N_1)$ [or equivalently, the fluctuation term $\xi(N_1)$ in Eq. (4)] of the roughly Gaussian profiles that one gets by vertically cutting through the contour plots of the net flux in Fig. 6; the measurements are given by the symbols, which have been connected to guide the eye. The magnitude of the fluctuations is seen to be highest around the symmetric distribution ($N_i=N/2$) and grows mildly with increasing driving frequency $f=50$, 55, 70 Hz. The thin fluctuating lines represent the quantity $2.8[F(N_1)+F(N_2)]^{1/2}$ [with $F(N_1)$ and $F(N_2)$ taken from Fig. 5], which follow the curves of $\sigma(N_1)$ reasonably well, in agreement with Eggers' prediction Eq. (7).

middle row). At the critical frequency itself, $M(N_i)$ becomes very flat and has an inflection point at the symmetric solution. At this point the two clustered states recombine with the symmetric state.

Above the critical frequency only this symmetric equilibrium survives (Fig. 6, bottom row), which is clearly stable now: For $N_1>N/2$ the averaged net flux is negative, depleting the compartment until the equilibrium at $N_1=N/2$ is reached. Equivalently for $N_1<N/2$ the average net flux is positive and the compartment will gain particles until $N_1=N/2$.

Also the *fluctuation term* $[\xi(N_i)]$ of the mapping in Eq. (4) can be obtained from Fig. 6. Making a cut in the vertical direction through the contour plots in the left column, the width of the distribution at any given value of N_i corresponds to the magnitude of the fluctuations at that point, i.e., to $\xi(N_i)$.

We find that the distributions along the vertical cuts follow an approximately Gaussian profile, with standard deviation

$$\sigma(N_i)=\sqrt{\langle G^2(N_i)-\langle G(N_i)\rangle^2\rangle}\equiv\xi(N_i). \tag{6}$$

The standard deviation $\sigma(N_i)$ is highest in the middle region (near $N_i=N/2$) as can be seen in Fig. 7, and decreases toward the sides. We also observe that $\sigma(N_i)$ grows with increasing frequency, though less strongly than the magnitude of the average flux (see Figs. 4 and 5). This is in agreement with our earlier observation that the relative influence of the fluctuations diminishes at high frequencies above the critical value f_c.

It is interesting to compare our results with the prediction of Eggers [3] concerning the amplitude of the fluctuations. He assumed that the particles passing from one compartment to the other are uncorrelated, which is equivalent to saying that $\xi(N_i)$ is uncorrelated Gaussian white noise [3,16]. Under this assumption the second moment is given by [cf. Eq. (8) in Ref. [3], properly integrated over time and normalized to hold for the actual particle numbers N_1 and $N_2=N-N_1$ instead of particle fractions]

$$\sigma^2(N_1)=K^2(f)[F(N_1)+F(N-N_1)], \tag{7}$$

with $K^2(f)$ a factor that may depend on the frequency f (but not on the total number of particles N). In Fig. 7 we see that this relation is satisfied reasonably well in our simulations, with $K^2(f)=2.8$ for each of the frequencies $f=50$, 55, 70 Hz.

IV. POTENTIAL FORMULATION

In order to quantify the relative influence of the terms $M(N_i)$ and $\xi(N_i)$, in this section we define a potential related to the average net flux $M(N_i)$. In the unclustered regime this potential has a single minimum at the symmetric distribution, whereas in the clustered regime it becomes a double-well potential with a barrier in the middle. By comparing the height of this barrier to the amplitude of the noise term $\xi(N_i)$, we have a direct measure for the relative importance of the fluctuations.

The average net flux $M(N_i)$ can be interpreted as a force, working toward one compartment. With this force one can associate a potential $V(N_i)$ as follows:

$$M(N_i)=-\frac{dV(N_i)}{dN_i}, \tag{8}$$

or equivalently,

$$V(N_i)=-\int_{N/2}^{N_i}M(N_i')dN_i'. \tag{9}$$

In Fig. 6 (right column) we have plotted the potentials corresponding to the average net fluxes (in the middle column). In fact, the raw net flux from the MD simulations (i.e., from the M depicted in Fig. 6) was fitted to a cubic polynomial, yielding a potential of the following general form:

$$V(N_i)=V_0+aN_i^2+bN_i^4. \tag{10}$$

The values of V_0, a, and b for each potential are given in the caption of Fig. 6.

For strong shaking ($f=70$ Hz, bottom) the potential has one single minimum at $N_i=150$, representing the stable symmetric state. Upon reducing the frequency, the bottom of the potential becomes flatter and flatter, giving the fluctuations ample opportunity to have a big effect on the particle numbers in each compartment. At the critical shaking frequency itself (close to $f=55$ Hz, middle) the minimum in the center becomes a maximum (the symmetric state becomes unstable) and the potential develops two wells corresponding to the clustered states. So in the clustered regime ($f=50$ Hz, top) the potential consists of two wells separated by a barrier in the middle.

As long as the amplitude of the fluctuations is larger than the height of the potential barrier, the clustering dynamics into either well will be interrupted (at irregular time intervals) by a statistical fluctuation that drives the system back to

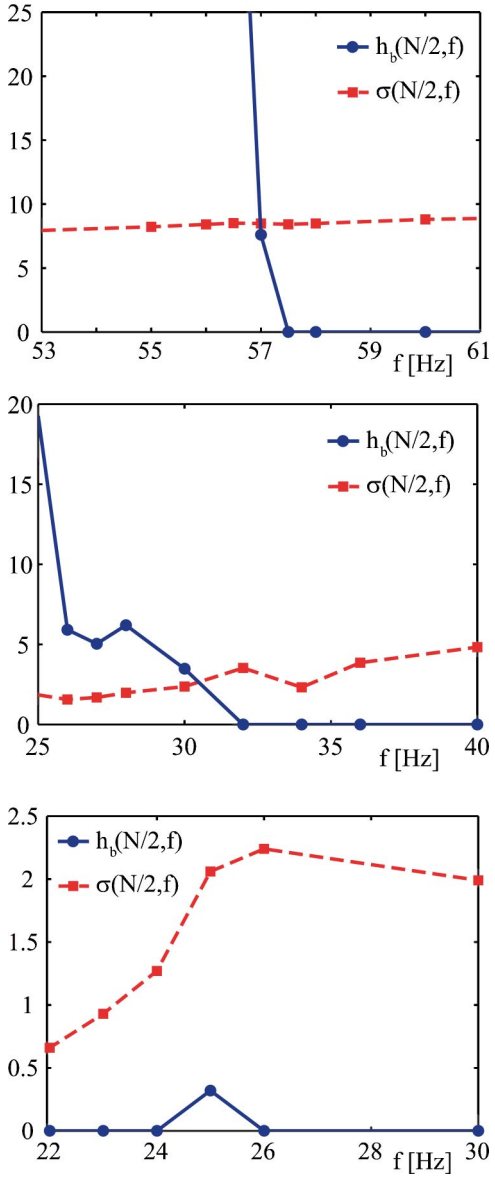

FIG. 8. (Color online) The amplitude of the fluctuations [represented by the maximal standard deviation $\sigma(N/2)$, i.e., $\xi(N/2)$, see Fig. 7; (red) squares connected by dashed line] and the height of the potential barrier $h_b(N/2)$ [cf. Fig. 6; (blue) dots connected by solid line] as functions of the driving frequency f, for $N=300$, 100, and 50 particles (top to bottom). There is a region below the critical frequency f_c (at which the barrier height becomes nonzero) where the fluctuations are still larger than the barrier height, which means that the system will switch intermittently from one potential well to the other, thus frustrating the mean-field behavior. The size of this region (and hence the overall influence of the fluctuations) grows for decreasing particle number N. For $N=50$ particles the fluctuations are seen to dominate at all frequencies.

the symmetric state (and from there again into any of the two wells). This is exactly the intermittent behavior that we observed in the MD simulations for frequencies just below the critical value f_c. In Fig. 8 the amplitude of the fluctuations is compared to the height of the potential barrier, as function of f, for $N=300$, 100, and 50 particles. It is seen that the region where the fluctuations are larger than the barrier grows with

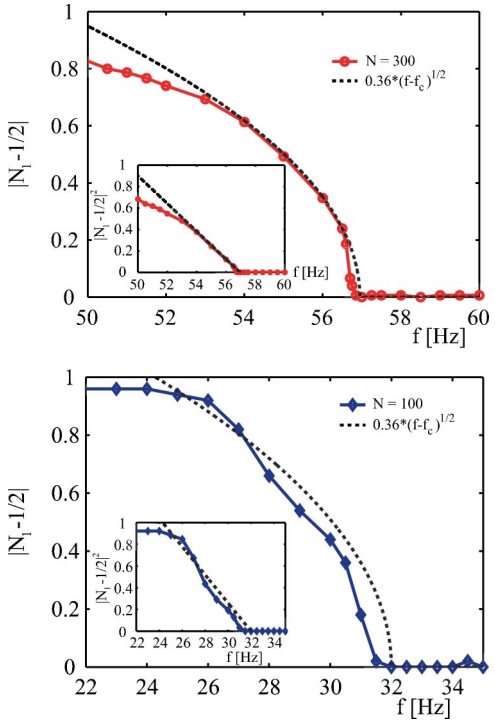

FIG. 9. (a) The bifurcation diagram for $N=300$ particles, driven at an amplitude of $a=1$ mm. Just below the critical frequency $f_c \approx 57$ Hz, the mean-field behavior (indicated by the dashed line) is slightly thwarted by the statistical fluctuations in the system. The inset shows the same diagram with the quantity along the vertical axis squared: the mean-field behavior now is represented by a straight line. (b) The same for $N=100$ particles. It is seen (also in the inset) that the mean-field behavior is much more disturbed than in (a).

decreasing total particle number N, just as expected.

When the driving frequency is reduced further below f_c, the height of the potential barrier increases (and at the same time the amplitude of the fluctuations decreases) until at a certain point the fluctuations are not able to kick the system out of the well anymore. It is at this point (for $N=300$ and 100 particles) that the mean-field behavior sets in. For $N=50$ the system never reaches such a point.

The situation is further illustrated in Fig. 9(a), which shows the bifurcation diagram for $N=300$ particles (cf. the backbone in Fig. 3, top): Just below the critical frequency f_c the points in this diagram do not follow the mean-field behavior [the dashed curve, branching off as $(f_c-f)^{1/2}$] but stay closer to the symmetric state. This is the result of the fact that the system still spends a considerable part of the time near the symmetric state, forced by the fluctuations. The mean-field behavior is seen to set in around $f=56.5$ Hz. This is illustrated also in the inset of Fig. 9(a), where the dashed straight line represents the mean-field prediction.

The deviations from the mean-field behavior are much more apparent for smaller values of N, as in Fig. 9(b) for $N=100$. Here the critical value lies around $f_c=32$ Hz, but the mean-field behavior is hidden in the noise until $f \approx 28$ Hz.

The same potential formulation can also be applied when the total number of particles is smaller. In Fig. 10 we show

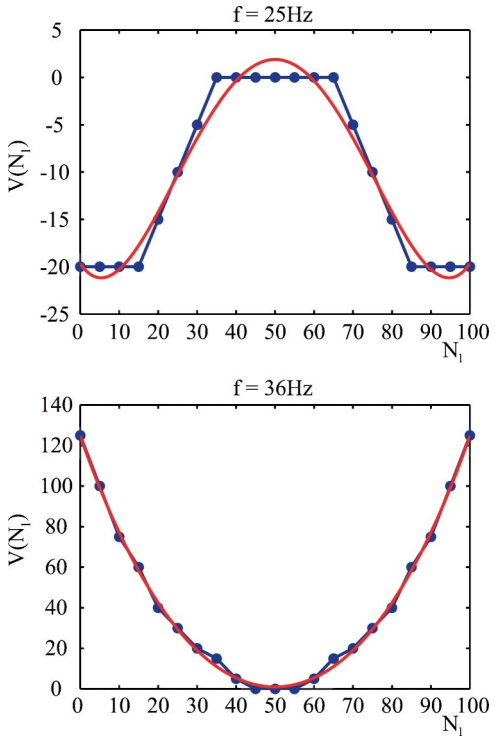

FIG. 10. The potential $V(N_i)$ for $N=100$ particles at mild shaking ($f=25$ Hz) and strong shaking ($f=36$ Hz), corresponding to the symmetric and clustered regimes, respectively (cf. Fig. 3, middle plot). The raw data from the average net flux have been fitted to a quartic polynomial as in Eq. (10); the coefficients $\{V_0,a,b\}$ are $\{1.90, -0.0231, 5.81\times10^{-6}\}$ for $f=25$ Hz, and $\{1.00, 0.0442, 2.14\times10^{-6}\}$ for $f=36$ Hz. At the critical frequency ($f_c\approx32$ Hz), the coefficient a goes through zero and the form of the potential changes from double well to single well.

two typical potentials for $N=100$ particles, at driving frequencies $f=25$ (clustered regime) and 36 Hz (symmetric regime). These have the same form as those for $f=50$ and 70 Hz with $N=300$ particles (see Fig. 6, rightmost column), but the absolute values differ considerably. In particular, the height of the potential barrier for $N=100$ is much smaller than for $N=300$, which means that it is much easier for the fluctuations to overcome it.

It may also be noted that the numerical data for $N=100$ are coarser than those for $N=300$. This is due to a practical complication at small particle numbers: the increased influence of the fluctuations makes it necessary to run the MD simulations for a much longer time before one obtains a reliable average net flux $M(N_i)$, needed for the potential $V(N_i)$. This problem becomes even worse for the case of $N=50$ particles.

V. TIME CORRELATION

A useful indicator for a phase transition in equilibrium statistical physics is the normalized time autocorrelation function $C(\tau)$ [10,14,17]

$$C(\tau)=\frac{\langle \delta n(t)\,\delta n(t+\tau)\rangle_t}{\langle \delta n^2(t)\rangle_t}, \tag{11}$$

where $\delta n(t)\equiv n(t)-\langle n(t)\rangle_t$ and the index t indicates that we take the temporal average. The function $C(\tau)$ is a measure of how correlated the signal $n(t)$ is to its value $n(t+\tau)$ a time τ later. It is 1 when the signal is totally correlated (for $\tau=0$), and fluctuates around zero when all correlations are lost. The typical lifetime of correlations in the signal τ_0 can be defined as the value of τ for which $C(\tau)$ becomes smaller than e^{-1} (≈0.37), corresponding to the standard mean-field form of the autocorrelation function $C_{\mathrm{mf}}(\tau)=e^{-\tau/\tau_0}$ [14,18,19]. Alternatively, one may define τ_0 via the slope of $C(\tau)$ as follows:

$$\frac{1}{\tau_0}=\left.-\frac{dC(\tau)}{d\tau}\right|_{\tau=0}, \tag{12}$$

which is the *decay rate* of the correlations at short time scales. Since we cannot take the validity of the mean-field approximation for granted here, we will use this second definition of τ_0.

For a standard second-order phase transition the lifetime τ_0 is known to diverge at the critical point, or equivalently, the inverse time scale $1/\tau_0$ (the decay rate of the correlations) goes to zero. We want to see to what extent this still holds for the clustering transition in our granular system, for decreasing values of the particle number N.

For this purpose, we have to determine averages over the time signal. This poses no difficulties in the regimes where the particles are either clearly clustered or not clustered at all, but in the intermittent regime just below the critical frequency (see Fig. 2, middle) the mean value $\langle n(t)\rangle$ [or equivalently, $\langle N_1(t)\rangle$] is an ambivalent quantity, since the particle numbers fluctuate between two different equilibrium points. That is why in this regime we work instead with the related quantity

$$\epsilon(t)=\left|\frac{N}{2}-N_1(t)\right|+\frac{N}{2}, \tag{13}$$

which makes all the data fluctuate around only one equilibrium point (namely, the upper one, between $N/2$ and N). The corresponding correlation function takes the form

$$C(\tau)=\frac{\langle \delta\epsilon(t)\,\delta\epsilon(t+\tau)\rangle_t}{\langle \delta\epsilon^2(t)\rangle_t}. \tag{14}$$

The result is depicted in Fig. 11 for $N=300$ particles. The autocorrelation goes from 1 downward, at different rates for different frequencies. As expected, the slowest decrease is observed for f around the critical frequency $f_c=56$–57 Hz.

From these curves, one can obtain the corresponding decay rates $1/\tau_0(f)$ [Eq. (12)] that are plotted in Fig. 12. This figure shows the decay rates not only for $N=300$ particles (top), but also for $N=100$ (middle) and $N=50$ (bottom). Below the critical frequency f_c we have evaluated $1/\tau_0$ both from the raw data [with $C(\tau)$ given by Eq. (11), solid stars] *and* from the intermittency-corrected data [with $C(\tau)$ as in Eq. (14), open stars]. As explained above, just below f_c one should work with the corrected, open symbols; for $f\ll f_c$ the

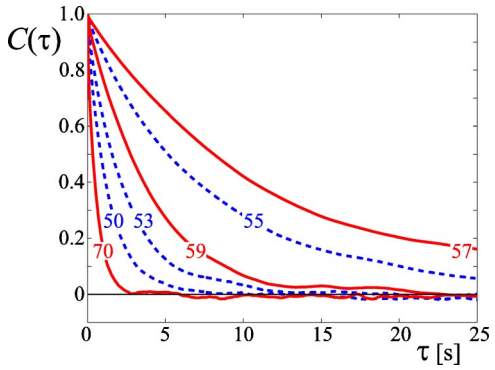

FIG. 11. The normalized autocorrelation function $C(\tau)$ for $N=300$ particles, for various driving frequencies f (indicated in the plot). The curves all decrease from the initial value 1, but at different rates depending on f. Close to the critical frequency $f_c \approx 56$–57 Hz the decay is slowest. The curves corresponding to $f < f_c$ are dashed, to distinguish them more easily from those for $f > f_c$ (solid lines).

intermittency disappears from the signal and the solid and open symbols simply coincide.

The standard behavior, namely, that $1/\tau_0$ goes to zero at the critical frequency, is still clearly present for $N=300$ (see the dashed lines). In fact, from this plot we get the most accurate but also the smallest value of the critical frequency f_c so far, namely, $f_c=55.7$ Hz.

The decay rate is seen to approach zero linearly, as $1/\tau_0 \propto |f-f_c|^\gamma$ with the critical exponent $\gamma=1$ known from mean-field theory [18]. In the symmetric regime ($f>f_c$) this linear behavior extends relatively far beyond the critical point, whereas in the clustered regime ($f<f_c$) it breaks down much more quickly. This is in agreement with the Landau theory for second-order phase transitions and is due to the nonlinearities that come into play as soon as the system moves away from the symmetric equilibrium [14,18,19].

Also for $N=100$ (Fig. 12, middle plot) the decay rate $1/\tau_0$ is still seen to tend to zero linearly at the critical point, which on the basis of this plot is estimated to lie at $f_c \approx 28.6$ Hz. This is considerably smaller than the value $f_c \approx 32$ Hz we had found earlier from the bifurcation diagram for $N=100$ in Figs. 3 and 9(b).

Finally, for $N=50$ particles (Fig. 12, bottom) the mean-field behavior breaks down, as expected. A proper determination of the critical point f_c is no longer possible from this plot, neither can one recognize the critical exponent γ.

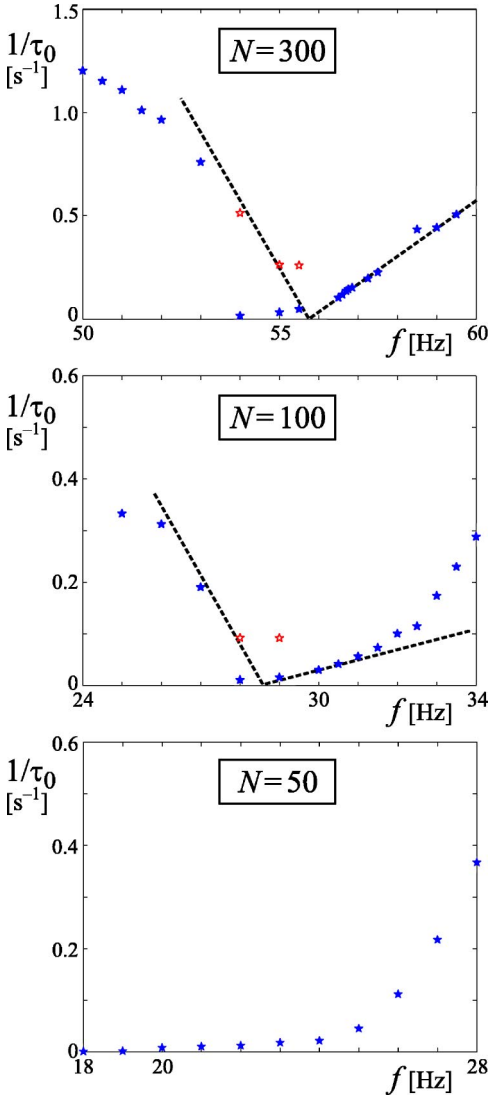

FIG. 12. (Color online) The correlation decay rates $1/\tau_0$ as function of the shaking frequency for $N=300$, 100, and 50 particles, respectively. The standard behavior of $1/\tau_0$ going to zero at the critical frequency f_c is still recognizable for $N=300$ and 100, but deteriorates for $N=50$. The plots for $N=300$ and 100 show that $1/\tau_0$ approaches zero linearly, i.e., as $|f_c-f|^\gamma$ with the mean-field critical exponent $\gamma=1$. The solid (blue) stars are based on the raw data; the open (red) ones have been corrected for the intermittency that occurs just below the critical point, according to the recipe given in the text [see Eqs. (13) and (14)].

VI. CONCLUSION

In conclusion, we have seen that statistical fluctuations profoundly influence the clustering behavior of a compartmentalized granular gas. As long as the number of particles (N) is sufficiently large, the clustering is seen to follow the lines of a standard second-order phase transition (i.e., a pitchfork bifurcation with critical exponent $\beta=1/2$). For smaller N, however, the enhanced influence of statistical fluctuations overwhelms the mean-field behavior, and the critical exponent cannot be determined anymore. We demonstrated this by means of bifurcation diagrams (Fig. 3) and also via the correlation time τ_0 at the clustering transition (Fig. 12).

In order to model the fluctuations in our system, we constructed the mapping (4) (describing the outflow of particles from a compartment per shaking cycle) in which the mean-field flux and the fluctuations appear as two separate terms. This separation enables us to directly compare the relative

importance of both contributions to the dynamics, and to study how the fluctuations start to dominate for decreasing particle number N.

Our results show that already at $N=300$ (i.e., much less than the 10^{23} particles of textbook statistical physics) mean-field results and the Eggers flux theory hold very nicely. Only for smaller N does the finite-number noise start to dominate, and the mean-field description breaks down.

ACKNOWLEDGMENTS

We wish to thank Professor Guenter Ahlers for a stimulating discussion on the autocorrelation function. This work is part of the research program of the Stichting Fundamenteel Onderzoek der Materie (FOM), which is financially supported by the Nederlandse Organisatie voor Wetenschappelijk Onderzoek (NWO); R.M. and D.v.d.M. acknowledge financial support.

[1] I. Goldhirsch and G. Zanetti, Phys. Rev. Lett. **70**, 1619 (1993).
[2] H. J. Schlichting and V. Nordmeier, MNU Math. Naturwiss. Unterr. **49**, 323 (1996).
[3] J. Eggers, Phys. Rev. Lett. **83**, 5322 (1999).
[4] K. van der Weele, D. van der Meer, M. Versluis, and D. Lohse, Europhys. Lett. **53**, 328 (2001).
[5] D. van der Meer, K. van der Weele, and D. Lohse, Phys. Rev. E **63**, 061304 (2001).
[6] D. van der Meer, K. van der Weele, and D. Lohse, Phys. Rev. Lett. **88**, 174302 (2002).
[7] A. Lipowski and M. Droz, Phys. Rev. E **65**, 031307 (2002).
[8] U. Marini Bettolo Marconi and A. Puglisi, Phys. Rev. E **68**, 031306 (2003).
[9] L. E. Reichl, *A Modern Course in Statistical Physics*, 2nd ed. (Wiley, New York, 1998).
[10] N. G. van Kampen, *Statistical Processes in Physics and Chemistry* (North-Holland Personal Library, Amsterdam, 1992).
[11] D. I. Goldman, J. B. Swift, and H. L. Swinney, Phys. Rev. Lett. **92**, 174302 (2004).
[12] J. J. Brey, F. Moreno, R. García-Rojo, and M. J. Ruiz-Montero, Phys. Rev. E **65**, 011305 (2001).
[13] A. Barrat and E. Trizac, Mol. Phys. **101**, 1713 (2003).
[14] P. M. Chaikin and T. C. Lubensky, *Principles of Condensed Matter Physics* (Cambridge University Press, Cambridge, U.K., 1995).
[15] In our MD simulations, the Eggers form of the flux function is retrieved in the limit of elastic wall collisions if we also use the original setup described by Eggers, with a narrow slit between the compartments instead of a finite wall.
[16] H. Risken, *The Fokker-Planck Equation* (Springer, Berlin, 1984).
[17] H. E. Stanley, *Introduction to Phase transitions and Critical Phenomena* (Oxford University Press, New York, 1971).
[18] S.-K. Ma, *Modern Theory of Critical Phenomena*, Frontiers in Physics Lecture Note Series Vol. 46 (W.A. Benjamin, Reading, MA, 1976).
[19] X.-L. Qiu and G. Ahlers, Phys. Rev. Lett. **94**, 087802 (2005).